Eur. Phys. J. Plus (2016) **131**: 120
DOI 10.1140/epjp/i2016-16120-9

THE EUROPEAN PHYSICAL JOURNAL PLUS

Regular Article

Adsorption of carbon monoxide on boroxol-ring-doped zigzag boron nitride nanotube: Electronic study via DFT

Ehsan Zahedi[1,a], Maryam Yari[2], and Hooman Bahmanpour[3]

[1] Department of Physical Chemistry, Shahrood Branch, Islamic Azad University, Shahrood, Iran
[2] Department of Chemical Engineering, Shahrood Branch, Islamic Azad University, Shahrood, Iran
[3] Department of Environmental Engineering, Shahrood Branch, Islamic Azad University, Shahrood, Iran

Received: 7 October 2015 / Revised: 2 March 2016
Published online: 27 April 2016 –

Abstract. Previous works have already demonstrated that reactivity and sensitivity of boron nitride nanotubes (BNNTs) toward gas molecules can be modified by impurity. In this work, three nitrogen atoms of BNNT $(7,0)$ are replaced with oxygen to study the adsorption of CO molecule through the surface of boroxol ring with different adsorption patterns, including side-on and end-on. All calculations have been done using the DFT-B3LYP/6-31G* level of theory, and their electronic energies are corrected by gCP and D3 correction terms. The calculated binding energies are large, which indicates that CO molecule undergoes chemical adsorption. NBO results showed that the charge transfer occurs from the tube to the gas molecule, which can slightly change the electronic properties of the tube. Density of state (DOS) and partial DOS (PDOS) analysis revealed that adsorption of CO molecule on the boroxol ring position is covalent in nature. The Laplacian of electron density, Lagrangian kinetic energy density, Hamiltonian kinetic energy density, and potential energy density at bond critical points between the tube and CO indicate that the interaction between the tube and CO molecule is covalent in nature. Topological analysis of the electron localization function shows that electrons in the new formed bonds are approximately localized, meaning that the nature of the adsorption process is chemical covalent.

1 Introduction

Air pollution caused by the release of chemical and particulate matter into the atmosphere is a real public health and environmental problem which can lead to global warming, acid rain, the deterioration of the ozone layer, etc. The U.S. Environmental Protection Agency (EPA) recommended Air Quality Index (AQI) for clean air based on the National Ambient Air Quality Standards (NAAQS) which mainly consists of ozone (O_3), particulate matter, carbon monoxide (CO), nitrogen oxides (NO_x), sulfur dioxide (SO_2), and lead (Pb) [1]. Carbon monoxide is a colorless, odorless, and tasteless gas emitted from the partial oxidation of carbon-containing compounds, photochemical reactions in the troposphere, volcanoes, forest fires, iron smelting, and normal animal metabolism. Carbon monoxide can reduce oxygen delivery to the body's organs through combination with hemoglobin and production of carboxyhemoglobin. A level of 50% of body's hemoglobin can be converted to the carboxyhemoglobin at a level of 700 ppm of CO, which can leads to seizure, coma, and fatality [2,3]. For protection of both public health and welfare, EPA assigned an AQI of 100 for carbon monoxide corresponds to a level of 9 ppm over 8 hours or 35 ppm over 1 hour [1]. Because of these adverse effects on health and the environment, studies focused on monitoring and/or filtering of carbon monoxide has promising potential and is the important issue of air cleaning. Interaction of environmental air pollutants on the external surface of different nanostructured materials is an attractive subfield due to potential applications in chemical sensors and filters. Adsorption of CO molecule on the nanostructured materials have been studied by different researchers experimentally [4–9] and theoretically [10–15]. The competitive candidates for interaction with CO are carbonaceous materials such as nanotubes, fullerenes, graphite, and diamond. It is well known that CO molecule is weakly physisorbed on carbonaceous surface especially pure nanotubes [16]. This unfavorable property may be enhanced by doping or functionalization of pure nanotubes. After the discovery of carbon nanotubes (CNTs), a numerous experimental and theoretical investigations have been dedicated to consider the capability of

[a] e-mail: e_zahedi@iau-shahrood.ac.ir (corresponding author)

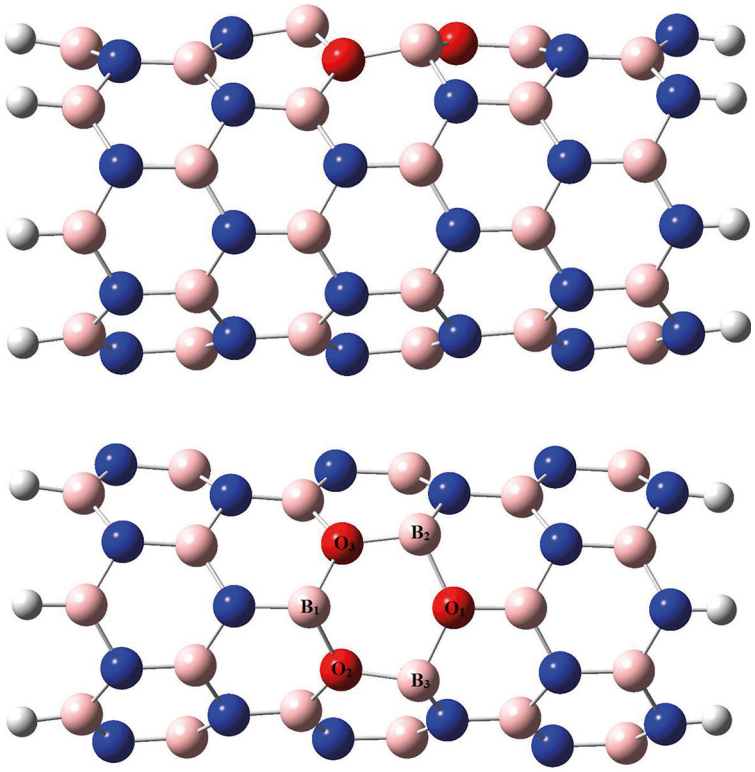

Fig. 1. Optimized geometry of oxygen-doped BNNT $(7,0)$ calculated at B3LYP/6-31G*.

boron nitride nanotubes (BNNTs) to detect gaseous molecules. BNNTs are more attractive respect to CNTs, because they are less toxic compared to CNTs and their electronic properties are dependent to the tube diameter and tube chirality [17]. Baierle *et al.* [18] and Wang *et al.* [19] showed that carbon monoxide is slightly adsorbed by a non-defective BNNT, but after substitutional doping the conductivity of BNNTs is increased and the reactivity of BNNT towards toxic gases is obviously improved [20–25]. Manipulation of nanotube structures has a weak point, it is very expensive. The natural impurity in the BNNTs can be the best choice to study the adsorption of gaseous molecules on tube surface. Fortunately, oxygen impurity is present naturally in all prepared BNNTs [26] and has been considered with different approaches. Experimental attempt by gentle plasma treatment shows that an oxygen plasma creates nitrogen vacancies that allow oxygen atoms to be successfully substituted onto the surface of BNNTs [27]. Electronic, magnetic and structural properties of oxygen-doped BNNTs have been studied theoretically by different researchers [28–31].

To the best of our knowledge neither calculations nor experimental investigations for adsorption of CO on oxygen-doped BNNTs have been reported. In this research adsorption sensitivity of oxygen-doped zigzag BNNT $(7,0)$ toward carbon monoxide is investigated using density functional theory (DFT) for the first time. This study can help in applications of oxygen-doped zigzag BNNT for sensing and/or filtering of CO.

2 Method of calculation

Adsorption of CO molecule toward oxygen-doped BNNT is studied using DFT method which is widely used for the study of molecular adsorbates on nanotubes. In the first step, single-walled $(7,0)$ boron nitride nanotube with length of 14 Å including 42 boron and 42 nitrogen atoms was constructed. Then two ends of the tube were saturated by 14 hydrogen atoms to avoid the boundary effects. Oxygen doping has been done on the selected BNNT by replacing three nitrogen atoms in the center of tube by three oxygen atoms to construct boroxol ring (fig. 1). In order to relax all atomic geometrical positions the structures, after and before adsorption process, were allowed to be optimized using Becke's three-parameter hybrid functional in combination with Lee-Yang-Parr correlation functional (B3LYP) [32,33], and 6-31G* basis set as implemented in the Gaussian 09 suite of program [34]. The B3LYP is an efficient and reliable method for prediction of ground state energy and the electronic structure of III-V semiconductors [35]. Recently, Grimme *et al.* [36] showed that London dispersion and basis set superposition error (BSSE) are two major shortcomings of the B3LYP/6-31G* method. Therefore in this study total electronic energies are corrected by using the B3LYP-gCP-D3/6-

Table 1. Calculated structural parameters (the distances are in angstrom) before and after adsorption of CO molecule on oxygen-doped BNNT $(7,0)$.

Bond type	Tube	Complex **A**	Complex **B**	Complex **C**
O.1-B.2	1.576	1.598	1.561	1.554
O.1-B.3	1.576	1.576	1.574	1.580
O.2-B.1	1.554	1.612	1.584	1.581
O.2-B.3	1.533	1.539	1.523	1.530
O.3-B.1	1.554	1.539	1.568	1.564
O.3-B.2	1.533	1.584	1.520	1.597
C-O	–	1.368	1.350	1.211

31G* method in which both corrections (gCP, D3) are directly added to the electronic DFT energy. It is important to mention that the gCP command corrects the intramolecular BSSE and the D3 command corrects missing dispersion energy through an atom-pairwise potential based on first principles data. Electron charge transfer (Q_{T}) from the nanotube to the adsorbate CO due to adsorption process have been calculated from NPA charges with the use of the NBO program version 3.1 (link 607, Gaussian 09) [37] at the same level of theory on the optimized structures. The total (TDOS), partial (PDOS), and overlap population (OPDOS) density of states have been created in terms of the Mulliken population analysis by convoluting the molecular orbital information with Gaussian curves of unit height and FWHM (Full Width at Half Maximum) of 0.3 eV [38]. Topological properties at bond critical points are investigated by using Multiwfn 3.3 program [39] on the calculated wave functions of optimized structures at the B3LYP/6-31G*. The wave functions for all studied structures are found to be stable under the perturbations considered by using STABLE keyword [40,41].

3 Results and discussion

In order to investigate the adsorption of CO molecule on the exterior surface of boroxol-ring-doped zigzag BNNT, oxygen doping for three nitrogen sites, $\mathrm{O_N}$, in the center of BN tube is considered. After optimization, two oxygen substitutional atoms are slightly displaced inward of the tube surface (fig. 1). The buckling effect is due to presence of mixture of sp^2 and sp^3 hybridization and repulsion between two lone electron pairs of oxygen atoms. Table 1 shows that upon relaxation, O-B bond lengths increase to 1.533, 1.554 and 1.576 Å, compared to the average B-N distance of 1.455 Å in pristine BNNT. Stability of bare oxygen-doped BNNT wave function was checked and its electronic state with doublet unrestricted open shell wave function was stable. In order to study the influence of O doping on the reactivity of the $(7,0)$ BN tube toward CO, different adsorption orientations relative to the boroxol ring surface (including side-on and end-on) are considered. After the geometry optimization, all different patterns were reduced to three configurations, which are given in fig. 2. Stability of their wave functions have been checked that are quartet, doublet and doublet unrestricted open shell for configurations **A**, **B** and **C**, respectively. The binding energies (E_b) for the adsorbed molecule and tube were defined as follows:

$$E_b = E_{\mathrm{Complex}}^{\mathrm{gCP\text{-}D3}} - E_{\mathrm{Tube}}^{\mathrm{gCP\text{-}D3}} - E_{\mathrm{CO}}^{\mathrm{gCP\text{-}D3}}$$

and

$$E^{\mathrm{gCP\text{-}D3}} = E^{\mathrm{el}} + E^{\mathrm{gCP}} + E^{\mathrm{D3}},$$

where $E_{\mathrm{Complex}}^{\mathrm{gCP\text{-}D3}}$ is the gCP-D3 corrected total energy of adsorbed CO molecule on the defected BN tube, $E_{\mathrm{Tube}}^{\mathrm{gCP\text{-}D3}}$ and $E_{\mathrm{CO}}^{\mathrm{gCP\text{-}D3}}$ are the gCP-D3 corrected total energy of the free tube and gas phase molecule, respectively.

The total electronic energies (E^{el}), gCP correction energies (E^{gCP}), D3 correction energies (E^{D3}) and binding energies are tabulated in table 2. In the all three investigated complexes, the adsorption processes are exothermic and chemical in nature. The end-on configuration from carbon atom of CO, configuration **C**, is the preferable configuration with binding energy −66.41 kcal/mol. Table 1 and fig. 2 indicate that the geometric structure of tube at the adsorption site are significantly deformed after the sorption of CO molecule. This is due to change in the local hybridization of

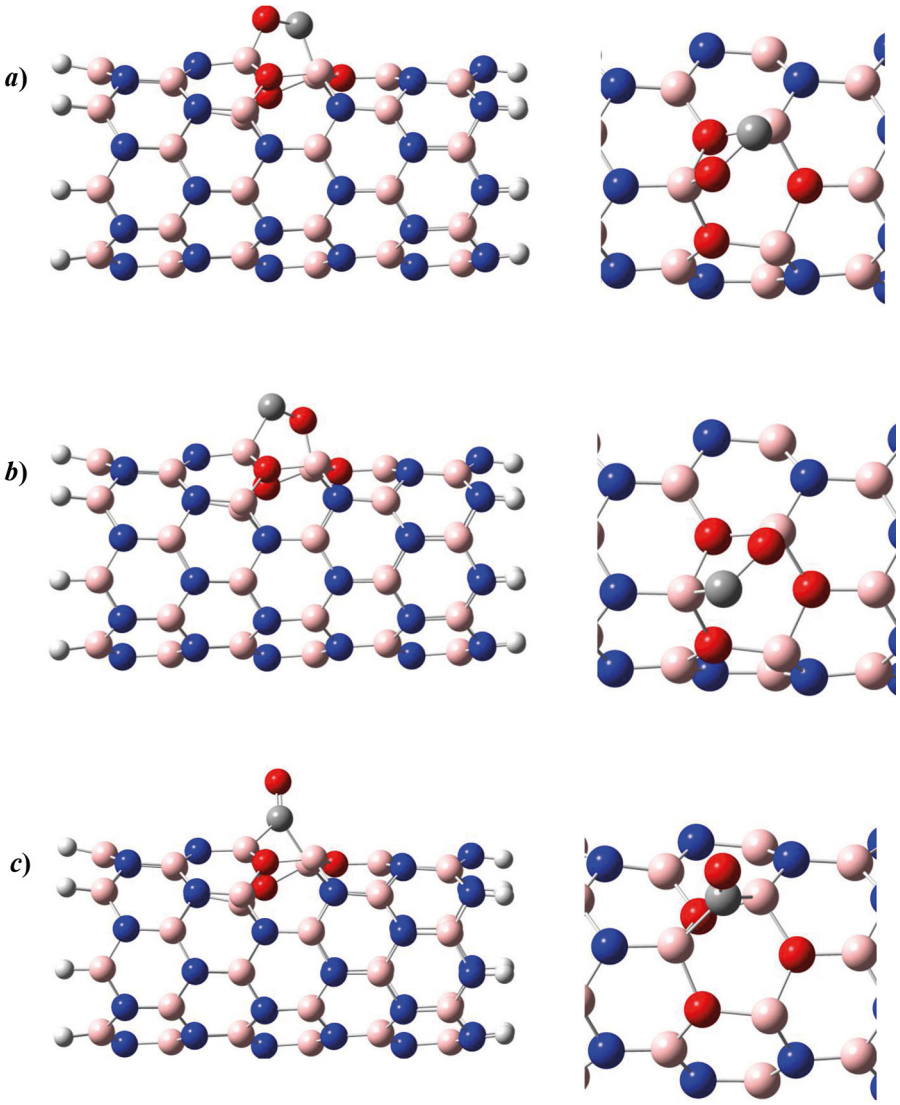

Fig. 2. Optimized geometry of three different CO adsorption orientations on the boroxol ring surface. (a) Configuration A, (b) Configuration B, and (c) Configuration C.

Table 2. Total electronic energies, gCP correction, D3 correction, binding energies and electron charge transfer for the adsorption of CO molecule on oxygen-doped BNNT $(7, 0)$.

Configuration	E_{el} (a.u.)	gCP correction (a.u.)	D3 correction (a.u.)	E_b (kcal/mol)	Q_T (el)[b]
CO	−113.309454336	0.0016310983	−0.00072773		
Tube	−3417.46574277	0.2464667137	−0.40954821		
Complex **A**	−3530.84339990	0.2569526796	−0.42145391	−44.25	−0.62
Complex **B**	−3530.86087673	0.2571870364	−0.42162195	−55.18	−0.66
Complex **C**	−3530.87639502	0.2544621678	−0.42128260	−66.41	−0.41

the boroxol ring atoms with a significant charge transfer (table 2) from the tube to the CO molecule. Electron charge transfer from the tube to the antibonding orbital CO-$2\pi^*$ leads to elongation of C-O bond (after adsorption process) from equilibrium value 1.137 Å in free form. One of important parameters for application of materials as sensor or

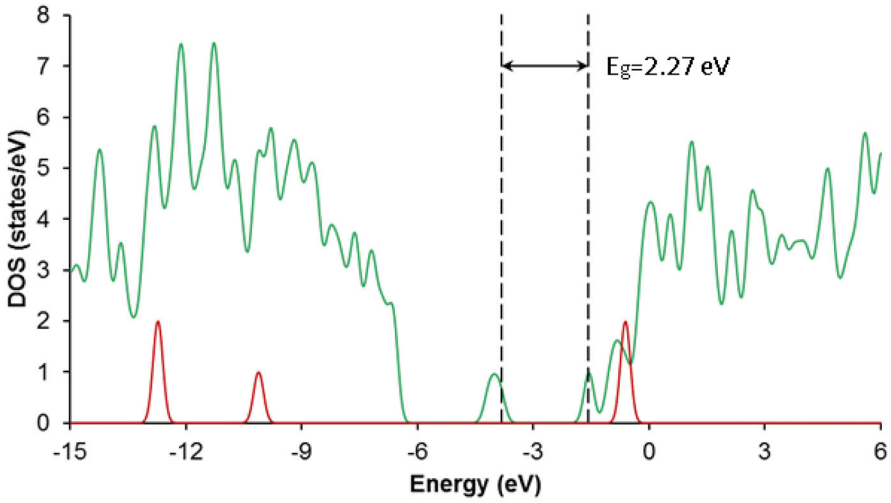

Fig. 3. Calculated total electronic density of state (TDOS) of tube (green), and CO (red) before adsorption. The dashed lines indicate the position of SOMO and LUMO states of the tube.

filter is recovery time which is based on the conventional transition state [42]:

$$\tau = \nu_0^{-1} e^{(-E_b/kT)},$$

where T is the temperature, k the Boltzmann constant and ν_0 the attempt frequency. Due to large binding energies of CO, long recovery time is expected. Therefore oxygen-doped BN tube cannot be repurified quite easily, meaning that is not favorable for CO gas detection but it can be used as an ideal material for elimination and filtering.

The nature of the bonding between adsorbent and adsorbate can be interpreted using molecular orbital compositions and their contributions to chemical bonding through DOS and OPDOS plots, respectively. The TDOS of a molecule at energy E can be written as

$$\mathrm{TDOS}(E) = \sum_i \delta\left(E - \varepsilon_i\right),$$

where ε is eigenvalue set of single-particle Hamilton and δ is Dirac delta function. Since, in the molecules energy levels are separate and individual, Dirac delta function can be replaced by Gaussian broadening function to get curve map of broadened DOS. The normalized Gaussian function is defined as

$$G(x) = \frac{1}{c\sqrt{2\pi}} e^{-\frac{x^2}{2c^2}},$$

where

$$c = \frac{\mathrm{FWHM}}{2\sqrt{2\ln 2}}.$$

In order to understand contribution of adsorbent and adsorbate fragments separately after sorption process, PDOS function of each fragments can be calculated as

$$\mathrm{PDOS}_A(E) = \sum_i \Xi_{i,A} G\left(E - \varepsilon_i\right),$$

where $\Xi_{i,A}$ is the composition of fragment A in orbital i, in such a manner that sum of $\mathrm{PDOS}_A(E)$ for all fragments gives $\mathrm{TDOS}(E)$. The OPDOS diagram for fragments A and B at energy E is calculated as

$$\mathrm{OPDOS}_{A,B}(E) = \sum_i X^i_{A,B} G\left(E - \varepsilon_i\right),$$

where $X^i_{A,B}$ is the composition of total cross term between fragments A and B in orbital i [39]. The TDOS spectra of bare oxygen-doped BN tube and CO gas molecule before adsorption are plotted in fig. 3. Presence of only one state of CO molecule near the LUMO state of bare tube, bring up possibility of slight changes in the electronic structure of tube after adsorption. For this purpose TDOS, and PDOS of tube and CO molecule after adsorption are investigated and presented in fig. 4. Band gap energy 2.27 eV for bare tube is changed by −0.14, +0.22 and +0.27 eV after adsorption process for complexes **A**, **B**, and **C**, respectively. As a result of adsorption singly occupied molecular orbital (SOMO) state of tube is dislocated from −3.83 eV to −3.89, −4.11 and −4.15 eV for complexes **A**, **B**, and **C**, respectively, while LUMO state is dislocated from −1.56 eV to −1.76, −1.62, and −1.61 eV. PDOS spectra of tube

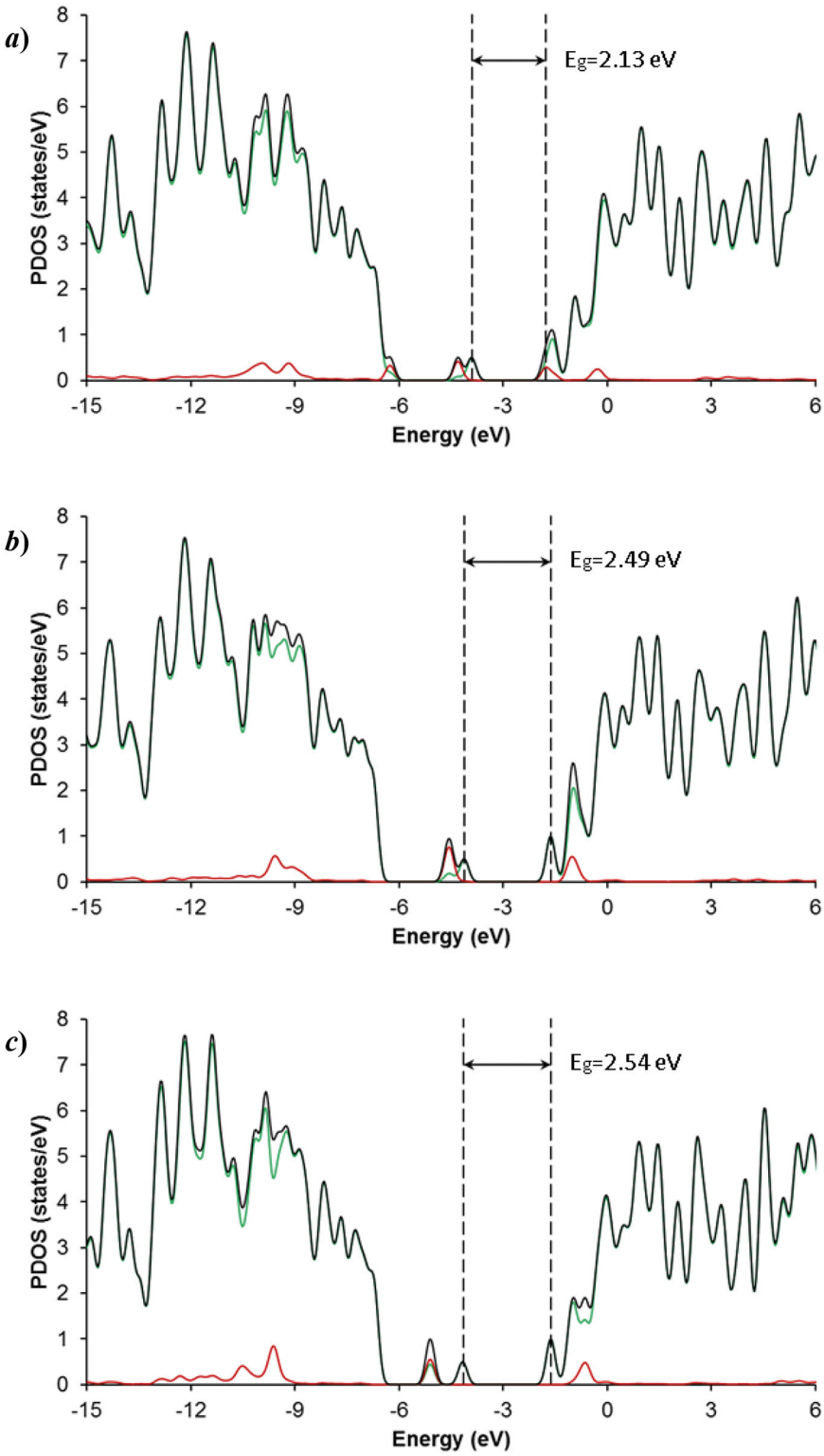

Fig. 4. Partial electronic density of state (PDOS) of tube (green), and CO (red) after adsorption, for (a) complex A, (b) complex B and (c) complex C. The dashed lines indicate the position of SOMO and LUMO states, and black curves represent total electronic density of state (TDOS) of each complex.

and CO molecule after adsorption showed that for complex **A** the LUMO state is composed of molecular orbitals of tube and CO molecule, while SOMO state is mainly due to molecular orbitals of tube. In the same way it is inferable that SOMO and LUMO states of complexes **B** and **C** are only due to the molecular orbitals of the tube.

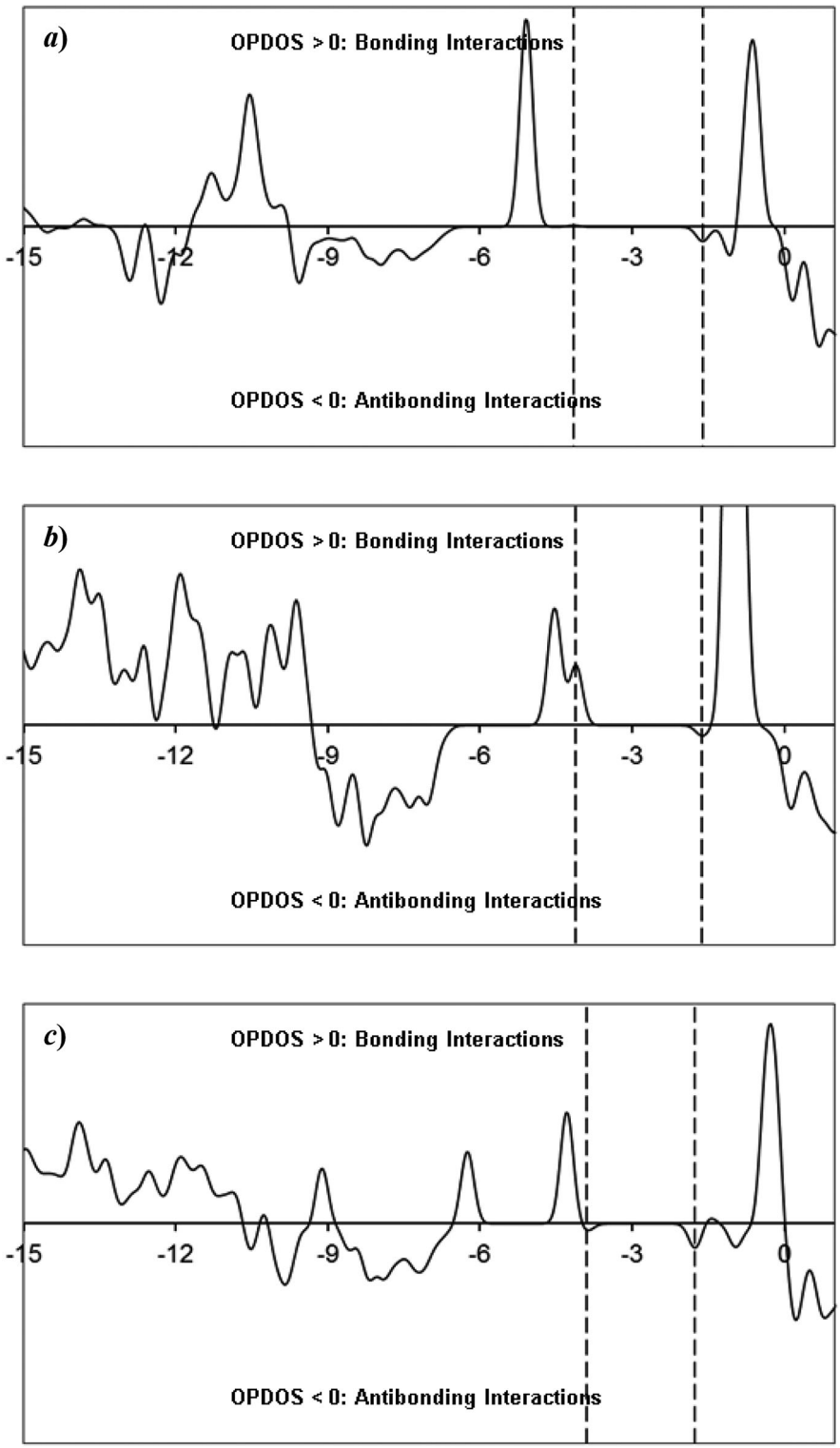

Fig. 5. Overlap population DOS curves between the tube and CO molecule, for (a) complex A, (b) complex B and (c) complex C.

Dislocation of molecular orbital states and changes in the band gap energy after adsorption of CO indicate that adsorption on the boroxol ring positions is covalent in nature. In the fig. 5, OPDOS diagrams of tube and CO fragments after adsorption shows that SOMO-1 state is favorable and conductive for forming chemical bond between tube and CO molecule in the complexes **A** and **C**, while for complex **B** the suitable state is SOMO.

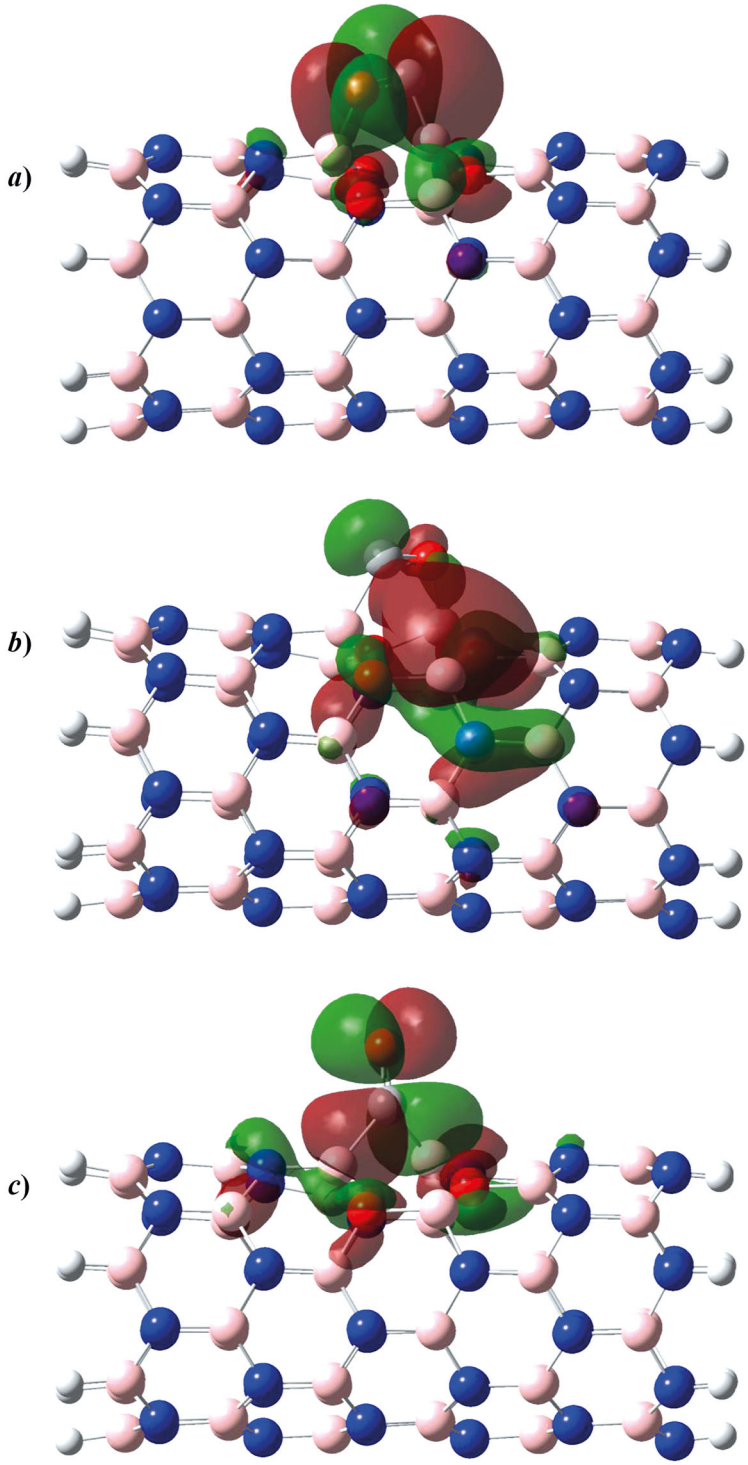

Fig. 6. Molecular projected self-consistent Hamiltonian (isovalue 0.02 a.u.) of (a) SOMO-1 state for complex A, (b) SOMO state for complex B and (c) SOMO-1 state for complex C.

To get better insight into the forming chemical bond between the tube and CO molecule, molecular projected self-consistent Hamiltonian of SOMO-1 state (−4.28 eV) of complex **A**, SOMO state of complex **B**, and SOMO-1 state (−5.08 eV) of complex **C** are visualized with isovalue 0.02 a.u., and presented in fig. 6. Since these molecular orbitals are occupied, presence of chemical bond between CO fragment and tube is inferable. The integration of the $\mathrm{OPDOS}_{A,B}(E)$

Table 3. The Lagrangian kinetic energy density, $G(\mathbf{r})$, Hamiltonian kinetic energy density, $K(\mathbf{r})$, potential energy density, $V(\mathbf{r})$, Laplacian of electron density, $\nabla^2\rho(\mathbf{r})$, and $|V(\mathbf{r})|/G(\mathbf{r})$ at bond critical points along bond line $(3,-1)$ calculated by QTAIM method at B3LYP/6-31G* level.

Configuration	Bond type	$G(\mathbf{r})$ (Hartree/a_o^3)	$K(\mathbf{r})$ (Hartree/a_o^3)	$V(\mathbf{r})$ (Hartree/a_o^3)	$\nabla^2\rho(\mathbf{r})$ (e/a_o^5)	$\lvert V(\mathbf{r})\rvert/G(\mathbf{r})$
Complex **A**	O-B_1	0.287392	0.131248	−0.418577	0.624325	1.456
	C-B_2	0.140111	0.184150	−0.324261	−0.176155	2.314
Complex **B**	C-B_1	0.088884	0.201975	−0.290860	−0.452362	3.272
	O-B_2	0.252464	0.133944	−0.386409	0.474079	1.530
Complex **C**	C-B_1	0.060077	0.169535	−0.229612	−0.437832	3.822
	C-B_2	0.070676	0.175145	−0.245821	−0.417876	3.478

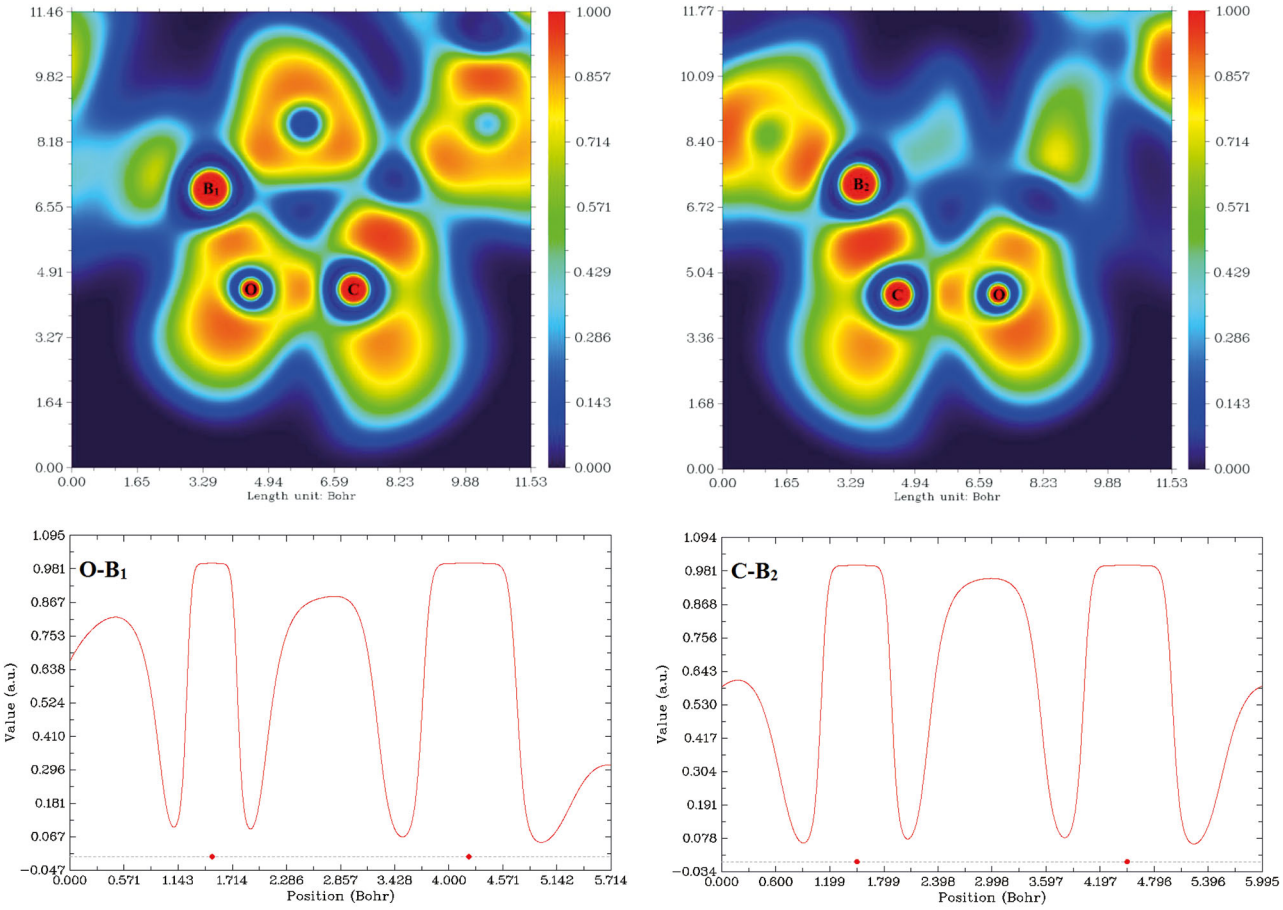

Fig. 7. Color-filled map and curve map of ELF for O-B_1 and C-B_2 bond paths of complex A.

function over all populated levels gives the total overlap population $\mathrm{TOP}_{A,B}$ between CO fragment and tube:

$$\begin{aligned}\mathrm{TOP}_{A,B}(E) &= \int_{-\infty}^{E_F} \mathrm{OPDOS}_{A,B}(E)\mathrm{d}E \\ &= \Delta E \sum_{\text{Occ. Orbitals}} \mathrm{OPDOS},\end{aligned}$$

where E_F is total chemical potential for electrons, and for isolated systems is equal to midway between HOMO and

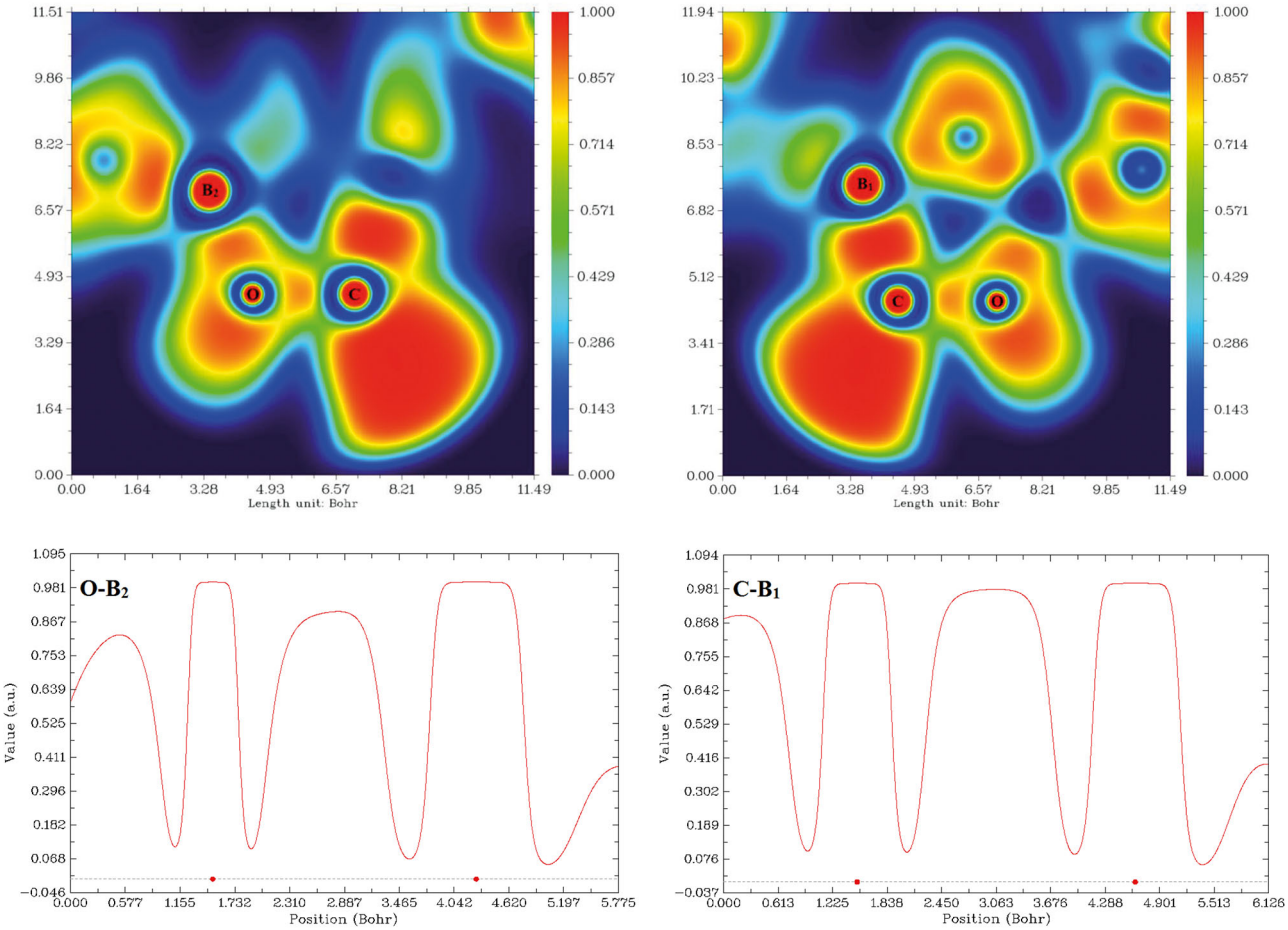

Fig. 8. Color-filled map and curve map of ELF for C-B_1 and O-B_2 bond paths of complex B.

LUMO energy levels. The calculated TOP values from -20 eV to the E_F are 0.089, 0.103 and 0.112 for complexes **A**, **B**, and **C**, respectively. This trend is in complete agreement with binding energies and indicates that complex **C** is the most stable configuration. It is not sufficient to trust to the density of states analysis for determination of interaction nature, therefore topological analysis of the electron density distribution $\rho(\mathbf{r})$ was used based on the quantum theory of AIM methodology for more assurance. The Laplacian of electron density, $\nabla^2\rho(\mathbf{r})$, Lagrangian kinetic energy density, $G(\mathbf{r})$, Hamiltonian kinetic energy density, $K(\mathbf{r})$, potential energy density, $V(\mathbf{r})$, and $|V(\mathbf{r})|/G(\mathbf{r})$ at bond critical points along bond line $(3,-1)$ give useful information about strength and characteristic of new formed bonds after adsorption of CO molecule. Lagrangian kinetic energy density and Hamiltonian kinetic energy density are directly related by Laplacian of electron density via local expression of the virial theorem at critical points [43]:

$$\frac{\hbar^2}{4m}\nabla^2\rho(\mathbf{r}) = G(\mathbf{r}) - K(\mathbf{r}),$$

and

$$V(\mathbf{r}) = -K(\mathbf{r}) - G(\mathbf{r}) = \frac{\hbar^2}{4m}\nabla^2\rho(\mathbf{r}) - 2G(\mathbf{r}).$$

If $2G(\mathbf{r}) > |V(\mathbf{r})| > G(\mathbf{r})$, positive value of $K(\mathbf{r})$ is associated with shared-electron (covalent) interaction, while zero or negative values denote closed-shell (electrostatic) or ionic interaction. Otherwise, negative and positive values of the Laplacian of electron density denote covalent and closed-shell interactions, respectively. As shown in table 3, $2G(\mathbf{r}) > |V(\mathbf{r})| > G(\mathbf{r})$ clause is observable for BCP of O-B_1 and O-B_2 bonds in complexes **A** and **B**, respectively. Positive $K(\mathbf{r})$ values 0.131248 and 0.133944 are obtained for above BCPs, which indicate that the nature of the mentioned bonds is covalent. For other interactions, valid parameter for determination of nature of interaction is the Laplacian of electron density, which are negative. Therefore, interaction of CO molecule with boroxol ring adsorption sites are covalent in nature, which is in agreement with density of states analysis. It has been demonstrated that a BCP with $|V(\mathbf{r})|/G(\mathbf{r}) < 1$, $1 < |V(\mathbf{r})|/G(\mathbf{r}) < 2$, and $|V(\mathbf{r})|/G(\mathbf{r}) > 2$ represent different types of interactions including

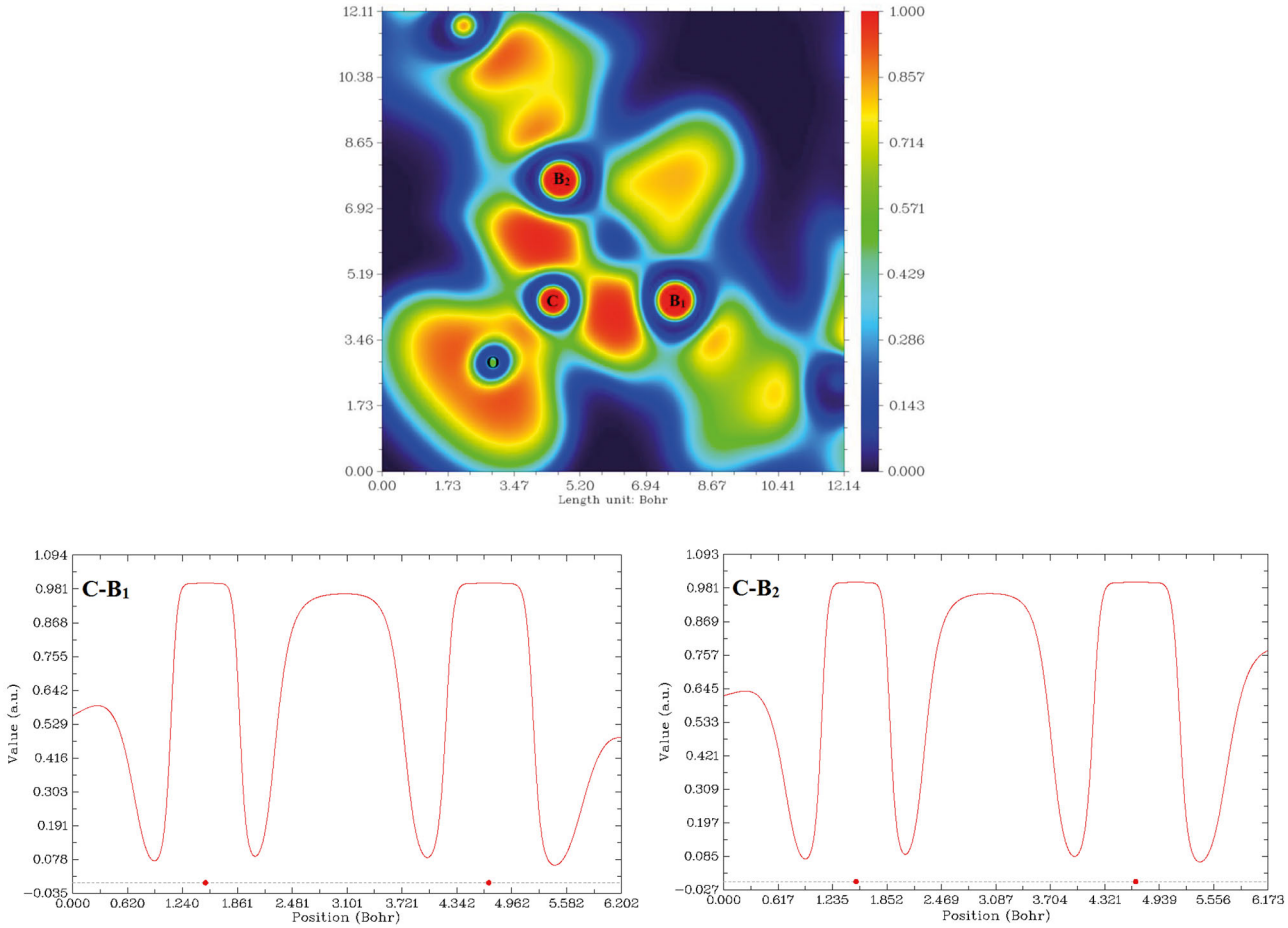

Fig. 9. Color-filled map and curve map of ELF for C-B_1 and C-B_2 bond paths of complex C.

pure closed-shell (CS), covalence, and strong shared covalence (SS), respectively [44]. $V(\mathbf{r})|/G(\mathbf{r})$ values for all new formed bonds confirm that O-B_1 bond in complex **A** and O-B_2 bond in complex **B** are covalent in nature, while in other new formed bonds the nature of interactions is strong shared covalence.

A topological analysis of the electron localization function (ELF) was performed in order to understand the nature of formed bonds between the tube and adsorbed gas. The electron localization function can be written as [45]

$$\mathrm{ELF} = \frac{1}{1 + (D(\mathbf{r})/D_0(\mathbf{r}))^2},$$

in which, $0 \leq \mathrm{ELF} \leq 1$, $D(\mathbf{r})$ and $D_0(\mathbf{r})$ are the excess kinetic energy density caused by Pauli repulsion, and Thomas-Fermi kinetic energy density, respectively. Maximum ELF value corresponds to the perfect localization and means that electrons are greatly localized. Color-filled maps and curve maps of ELF for the bond formed between the tube and CO molecule after adsorption process are sketched in figs. 7–9. In fig. 7, color-filled maps of complex **A** show that electrons in C-B_2 bond are more localized than O-B_1 bond. It is clear from curve maps of ELF that maximum value of ELF between C and B_2 atoms is 0.96 while maximum value of ELF between O and B_1 atoms is about 0.90. Color-filled maps of fig. 8 reveals that in complex **B** electrons in C-B_1 bond is more localized than O-B_2. For these bonds, curve maps of ELF are presented and state that maximum value of ELF function between C and B_1 is more than 0.98, but maximum value of ELF function between O and B_2 is about 0.90. Color-filled map of complex **C** in fig. 9 reveals that C atom of CO is bonded to the both B_1 and B_2 atoms of tube. Curve maps of ELF for C-B_1 and C-B_2 bonds indicate that electrons between these atoms are highly localized and ELF value for both bonds is about 0.98. In all configurations electron localization function for each of new formed bonds is larger than 0.9, meaning that after adsorption of CO gas on the adsorption sites of boroxol ring surface strong chemical covalent bonds are formed which is in complete agreement with energetic and electronic results.

4 Conclusion

In summary, the adsorption capability of oxygen-doped BNNT $(7, 0)$ toward carbon monoxide with different orientation to the boroxol ring surface (including side-on and end-on) is investigated using the B3LYP/6-31G* level of theory. The oxygen defect for three nitrogen sites was used to tailor the physical and chemical properties of the raw BNNT. The gCP-D3 corrected binding energies revealed that the studied tube is reactive toward CO molecule. DOS and PDOS results showed that electronic properties of the tube is not very sensitive to the adsorption of CO molecule, therefore the tube can be used as suitable filter to eliminate the gas molecule. Topological analysis of the electron density distribution and electron localization function are unanimous that the adsorption process is chemical covalent in nature due to localized electrons in the new formed bonds.

References

1. Air Pollution Monitoring (U.S. Environmental Protection Agency), `http://www3.epa.gov/airquality/montring.html`.
2. P. Tikuisis, D.M. Kane, T.M. McLellan, F. Buick, S.M. Fairburn, J. Appl. Physiol. **72**, 1311 (1992).
3. OSHA fact sheet, *Carbon monoxide poisining* (U.S. Department of Labor, Occupational Safety and Health Administration, 2002).
4. M. Cho, C. Hess, M. Bonn, Phys. Rev. B **65**, 205423 (2002).
5. M. Kawai, Bull. Mater. Sci. **20**, 769 (1997).
6. G.P. Lithoxoos, A. Labropoulos, L.D. Peristeras, N. Kanellopoulos, J. Samios, I.G. Economou, J. Supercrit. Fluids **55**, 510 (2010).
7. M. Rubeš, L. Grajciar, O. Bludský, A.D. Wiersum, P.L. Llewellyn, P. Nachtigall, Chem. Phys. Chem. **13**, 488 (2012).
8. S. Santucci, S. Picozzi, F.D. Gregorio, L. Lozzi, C. Cantalini, L. Valentini, J.M. Kenny, B. Delley, J. Chem. Phys. **119**, 10904 (2003).
9. I. Voleská, P. Nachtigall, E. Ivanova, K. Hadjiivanov, R. Bulánek, Catal. Today **243**, 53 (2015).
10. O. Leenaerts, B. Partoens, F.M. Peeters, Phys. Rev. B **77**, 125416 (2008).
11. A.A. EL-Barbary, G.H. Ismail, A.M. Babeer, J. Surf. Eng. Mater. Adv. Technol. **3**, 287 (2013).
12. V. Nagarajan, R. Chandiramouli, Superlattices Microstruct. **78**, 22 (2015).
13. P.N. Samanta, K.K. Das, Chem. Phys. Lett. **577**, 107 (2013).
14. P.N. Samanta, K.K. Das, RSC Adv. **4**, 59056 (2014).
15. X.R. Shi, J. Wang, K. Hermann, J. Phys. Chem. C **114**, 13630 (2010).
16. J.F. Espinal, A. Montoya, F. Mondragon, T.N. Truong, J. Phys. Chem. B **108**, 1003 (2004).
17. J.F. Jia, H.S. Wu, H. Jiao, Physica B **381**, 90 (2006).
18. R.J. Baierle, T.M. Schmidt, A. Fazzio, Solid State Commun. **142**, 49 (2007).
19. R. Wang, D. Zhang, Aust. J. Chem. **6**, 941 (2008).
20. P. Piquini, R.J. Baierle, T.M. Schmidt, A. Fazzio, Nanotechnology **16**, 827 (2005).
21. T.M. Schmidt, R.J. Baierle, P. Piquini, A. Fazzio, Phys. Rev. B **67**, 113407 (2003).
22. R.J. Baierle, P. Piquini, T.M. Schmidt, A. Fazzio, J. Phys. Chem. B **110**, 21184 (2006).
23. R.X. Wang, R.X. Zhu, D.J. Zhang, Chem. Phys. Lett. **467**, 131 (2008).
24. R. Wang, D. Zhang, Y. Liu, C. Liu, Nanotechnology **20**, 505704 (2009).
25. J. Zhang, K.P. Loh, J.W. Zheng, M.B. Sullivan, P. Wu, Phys. Rev. B **75**, 245301 (2007).
26. S.S. Batsanov, A.S. Batsanov, *Introduction to structural chemistry* (Springer, Dordrecht, 2012).
27. X.J. Dai, Y. Chen, Z. Chen, P.R. Lamb, L.H. Li, J.D. Plessis, D.G. McCulloch, X. Wang, Nanotechnology **22**, 245301 (2011).
28. A. Boshra, A. Seif, Can. J. Phys. **87**, 647 (2009).
29. A. Seif, A. Boshra, J. Mol. Struct. (THEOCHEM) **895**, 96 (2009).
30. L.D.A. Silva, S.C. Guerini, V. Lemos, J.M. Filho, IEEE Trans. Nanotech. **5**, 517 (2006).
31. J. Wu, W. Zhang, Solid State Commun. **149**, 486 (2009).
32. A.D. Becke, J. Chem. Phys. **98**, 5648 (1993).
33. P.J. Stephens, F.J. Devlin, C.F. Chabalowski, M.J. Frisch, J. Phys. Chem. **98**, 11623 (1994).
34. M.J. Frisch, G.W. Trucks, H.B. Schlegel, G.E. Scuseria, M.A. Robb, J.R. Cheeseman, G. Scalmani, V. Barone, B. Mennucci, G.A. Petersson, H. Nakatsuji, M. Caricato, X. Li, H.P. Hratchian, A.F. Izmaylov, J. Bloino, G. Zheng, J.L. Sonnenberg, M. Hada, M. Ehara, K. Toyota, R. Fukuda, J. Hasegawa, M. Ishida, T. Nakajima, Y. Honda, O. Kitao, H. Nakai, T. Vreven, J.A. Montgomery-Jr., J.E. Peralta, F. Ogliaro, M. Bearpar, J.J. Heyd, E. Brothers, K.N. Kudin, V.N. Staroverov, R. Kobayashi, J. Normand, K. Raghavachari, A. Rendell, J.C. Burant, S.S. Iyengar, J. Tomasi, M. Cossi, N. Rega, J.M. Millam, M. Klene, J.E. Knox, J.B. Cross, V. Bakken, C. Adamo, J. Jaramillo, R. Gomperts, R.E. Stratmann, O. Yazyev, A.J. Austin, R. Cammi, C. Pomelli, J.W. Ochterski, R.L. Martin, K. Morokuma, V.G. Zakrzewski, G.A. Voth, P. Salvador, J.J. Dannenberg, S. Dapprich, A.D. Daniels, O. Farkas, J.B. Foresman, J.V. Ortiz, J. Cioslowski, D.J. Fox, Gaussian 09, Revision A.02-SMP (Gaussian, Inc., Wallingford CT, 2009).
35. S. Tomic, B. Montanari, N.M. Harrison, Physica E **40**, 2125 (2008).
36. H. Kruse, L. Goerigk, S. Grimme, J. Org. Chem. **77**, 10824 (2012).

37. E.D. Glendening, A.E. Reed, J.E. Carpenter, F. Weinhold, NBO Version 3.1.
38. N.M. O'Boyle, A.L. Tenderholt, K.M. Langner, J. Comp. Chem. **29**, 839 (2008).
39. T. Lu, F. Chen, J. Comp. Chem. **33**, 580 (2012).
40. M.H. Gordon, J.A. Pople, J. Chem. Phys. **89**, 5777 (1988).
41. G.G. Hall, Philos. Mag. **6**, 249 (1961).
42. E. Zahedi, Physica B **407**, 3841 (2012).
43. E. Zahedi, C. R. Chim. **16**, 189 (2013).
44. E. Espinosa, I. Alkorta, J. Elguero, E. Molins, J. Chem. Phys. **117**, 5529 (2002).
45. B. Silvi, A. Savin, Mineral Mag. A **58**, 842 (1994).